Behaviour of dopants in gold-based metallizations to GaAs

A. PIOTROWSKA[1)], E. KAMIŃSKA[1)], X. W. LIN[2)], Z. LILIENTAL-WEBER[2)], J. WASHBURN[2,3)], E. WEBER[3)], A.J. BARCZ[1)], S. GIERLOTKA[1,4)], S. KWIATKOWSKI[5)]

[1)] Institute of Electron Technology, Division of Optoelectronics
al. Lotników 46, 02-668 Warszawa, Poland
[2)] Materials Science Division, Lawrence Berkeley Laboratory
University of California, Berkeley, CA 94720, USA
[3)] Department of Materials Science and Mineral Engineering
University of California, Berkeley, CA 94720, USA
[4)] High Pressure Research Center, Polish Academy of Sciences
Sokołowska 29, 01-142 Warszawa, Poland
[5)] Soltan Institute for Nuclear Studies
Hoża 69, 00-681 Warszawa, Poland

1. Introduction

Modern device concepts strongly depend on reliable and well controlled electrical contacts through which we have to communicate with the interior of the device from the outside world. In particular, III–V semiconductor devices for both the optoelectronic and the high speed digital and analog applications can be fully exploited only with adequate ohmic contacts. The most common approach for making ohmic contacts for these devices involves the use of gold-based metallizations, heat treated for a short time at temperatures in the range $400 \div 500$ °C. The contact schemes are designed to supply a suitable dopant and possibly an additional element improving contact adhesion and/or its morphology [1÷3].

The general picture explaining ohmic character of gold-based contacts is that the heat treatment drives the dopant from the metallization into the underlying semiconductor, significantly decreasing the thickness of metal/semiconductor potential barrier, so that carriers may tunnel through it in the field emission regime. The metallurgy of gold-based contacts, however, has been found to be complex chemically, sensitive to the wide range of parameters (e.g. surface cleaning, composition and thickness of contacting layers, order of evaporation, annealing temperature and time, annealing environment, heating and cooling rate) and the understanding of the basic process which determines ohmic behaviour is still far from satisfactory [4÷6]. One of the crucial questions concerns the behavior of doping species during contact annealing and the mechanism through which they participate in the formation of low resistivity contacts. While the model of tunneling applied to ohmic contact seems very reasonable, heavy doping at the metal/GaAs interface has not been experimentally detected. Moreover, the formation of crystalline heterojunction (graded or abrupt) or highly disordered interfacial layer could provide alternative explanations of ohmic behaviour. The crystalline heterojunction model postulates the reduction of the metal/semiconductor barrier height; other mechanisms responsible for ohmic properties involve hopping between the gap states or recombination through trap states [7÷13].

To extend the knowledge on the nature of ohmic contacts and to get better understanding on the role of doping elements in the formation of ohmic contacts to GaAs, a comparative study of the annealing behaviour of Au(Zn)/*p*-GaAs, Au(Ge)/*n*-GaAs, and Au(Te)/*n*-GaAs metallizations has been carried out in this work. The layout of the experiment was based on two premises. First, we have chosen dopants which are electrically active when placed in GaAs lattice on specific sites: Zn needs Ga sites, Te requires As vacancies, Ge as an amphoteric dopant can substitute for As or Ga sites. Second, we intended to alter the composition of the surface region of GaAs by using different annealing conditions. Since the decomposition of GaAs in contact with Au strongly depends on whether the system is open or closed during heat treatment, contacts were annealed in two configurations, either with or without an encapsulating layer. In an open system the reaction of Au with GaAs proceeds through entropy – driven evaporation of arsenic accompanied by a migration of gallium atoms into the Au film [14]. It is expected that in this configuration both Ga and As sites are available for doping elements.

Annealing with a capping layer has been shown to suppress the sublimation of As from the contact region [15, 16] and to reduce the extent of contact reaction. It is expected that in this configuration Au/GaAs reaction creates preferentially Ga vacancies. There is a certain solubility of Ga in Au which, at the temperature typical for ohmic contact formation, can approach several tenths of an atomic percent [17÷19]. These Ga vacancies would serve for Zn and Ge atoms to form acceptors and donors, respectively. As for arsenic, which is insoluble in Au, it can accumulate at the metal/GaAs interface and/or create antisite As_{Ga} defects. Thus, annealing under capping layer may reduce the Ga availability of the As vacancies in the GaAs/Au interfacial region, and Te atoms would serve as a probe of the accessibility of such sites.

2. Experimental procedure

Contacts were formed on (001) GaAs wafers subjected to chemical cleaning and etching in $NH_4OH - H_2O_2 - H_2O$ prior to deposition of the contact materials. *n*-GaAs substrates doped with Te to $n = 7 \cdot 10^{17}$ cm^{-3} were used for Au(Te) or Au(Ge), while *p*-GaAs, doped with Zn to $p = 1.2 \cdot 10^{18}$ cm^{-3} was used for Au(Zn). Metallizations were deposited in oil-free vacuum at pressure 10^{-7} Tr. Sequential evaporation from resistive heated crucibles was performed for Au(Te) and Au(Zn), in order to produce a sandwich structures with the thicknesses 130 nm Au/20 nm Te/20 nm Au/*n*-GaAs and 270 nm Au/40 nm Zn/ /40 nm Au/*p*-GaAs, respectively. The contact metallization Au(Ge), 300 nm thick was prepared using Au-8 wt.% Ge alloy source. Capping layers of SiO_2 or Al_2O_3, 200 nm thick, were deposited by RF magnetron sputtering with power densities of 7 W/cm² or 9 W/cm², at a pressure of $4 \cdot 10^{-3}$ Tr, and background pressure better than 10^{-6} Tr. They were removed after contact annealing by wet etching: SiO_2 was dissolved in buffered HF, Al_2O_3 in KOH solution.

The metallized samples of large area were prepared for metallurgical studies; the patterned samples for electrical measurements were prepared by standard photolithographic techniques. They included subtractive etching of a positive contact structure in 10% $CH_4N_2S-HCl-15\%\ H_2O_2=20:1:1$ solution.

Heat treatments were carried out by furnace annealing under flowing H_2 at temperatures from 320 to 480°C. The duration of annealing was 3 minutes.

The electrical characterization involved measuring the Schottky barrier height Φ_B for rectifying junctions and the specific contact resistance r_c for ohmic contacts. Φ_B was determined from forward-biased current-voltage (I−V) characteristics; a four-point method [20] was used to evaluate r_c.

The techniques used in the study of metallurgical properties included Rutherford backscattering (RBS) and secondary ion mass spectroscopy (SIMS) to probe composition profiles, X-ray diffraction (XRD) to identify phases and their preferred orientations, and transmission electron microscopy (TEM) to investigate the microstructure of contact region. In view of the expected sublimation of volatile components of the contact system during heat treatment, a thin-film collector method was applied to measure their evaporative losses. While each of the applied techniques presents certain disadvantages (i.e. relatively poor lateral resolution of SIMS and RBS and overlap of signals in RBS spectra, limited sensitivity of XRD in detection of small quantities of a crystalline phase at the interface, problems related to the thinning of the samples to electron transparency in TEM), all they provide a consistent picture of contact microstructure when taken together.

The XRD experiments were performed using Cu K_α radiation with Siemens D500 diffractometer equipped with quartz monochromator and position sensitive detector (PSD). The X-ray beam was incident onto a sample at a constant angle of 5°, while the sample was rotating around the surface normal during measurements. The TEM observations were made on both plan-view and cross-sectional specimens. The plan-view specimens were prepared by chemical etching, followed by ion milling, while the cross-sectional specimens were prepared by ion milling with the specimen surface being perpendicular to the GaAs [110] direction. A JEOL 200CX high-resolution electron microscope (HREM) operating at 200 kV and the Atomic Resolution Microscope at Berkeley operating at 800 kV were employed in this study. RBS measurements were performed using 2 MeV $^4He^+$ ion beam produced by Van de Graff accelerator and an experimental setup at the Institute for Nuclear Studies at Warsaw. SIMS profiling was performed with a 4 keV Ar^+ primary beam scanned over a relatively large crater of 2×2 mm. Electronic diaphragm was adjusted to detect secondary ions from the central region of 0.5×0.5 mm.

Measurements of arsenic loss were carried out by a thin-film collector method [16]. Collectors for capturing the evaporative species consisted of 100 nm thick Cr film deposited by DC magnetron sputtering onto Si/SiO_2 substrates. They were cut to the same size as the metallized GaAs samples and placed, face-to-face, on the top of them during thermal processing. After annealing, the composition of the Cr collector film was analysed by RBS. The number of atoms of an element trapped per unit area was determined from the ratio of the integrated yield in its respective peak to the integrated yield in the Cr peak.

3. Results and discussion

3.1. Electrical properties

All the as-deposited contacts behave as Schottky barriers with heights of 0.4 eV, 0.88 eV and 0.9 eV for *p*-GaAs/Au(Zn), *n*-GaAs/Au(Te) and *n*-GaAs/Au(Ge), contacts, respectively. Another observation common for all contacts is that any heat treatment degrade their rectifying properties. However, a striking difference between electrical behaviour of annealed Au(Te) contacts and other ohmic contact metallizations has been found. While both *p*-GaAs/Au(Zn) and *n*-GaAs/Au(Ge) contacts exhibit excellent ohmic properties when annealed with insulating cap, *n*-GaAs/Au(Te) structures form rectifying contacts over the entire range of processing temperatures. The barrier height decreased to 0.8 eV upon heat treatment at 420 °C; after the annealing at 480°C the contacts still preserved a nonlinear $I-V$ characteristics. The annealing behavior of capless *n*-GaAs/Au(Te), *p*-GaAs/Au(Zn) and *n*-GaAs/(AuGe) structures is similar to other gold-based metallizations where heat treatment is necessary to form ohmic contact and the specific contact resistance exhibits a minimum as a function of the annealing temperature. Figs. 1÷3 display the corresponding dependence of the specific contact resistance on the temperature of heat treatment. It is worth noting that for GaAs/Au(Zn) metallization annealing with a capping layer broadens the process window in the ohmic contact formation and slightly lowers the specific contact resistance. The r_c reaches the minimum value at a temperature around 420°C.

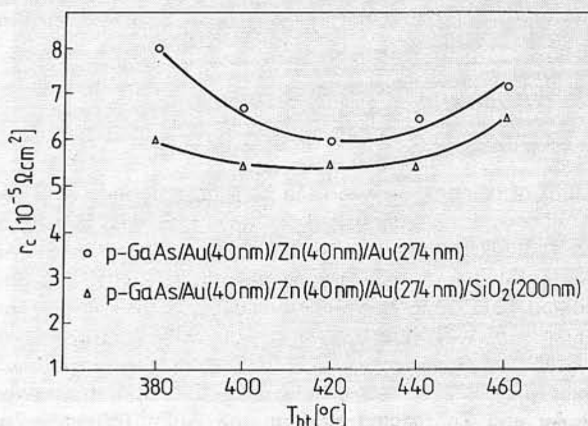

Fig. 1. Dependence of the specific contact resistance of GaAs/ /Au (40 nm)/Zn(40 nm)/Au (274 nm) contacts on the temperature of heat treatment

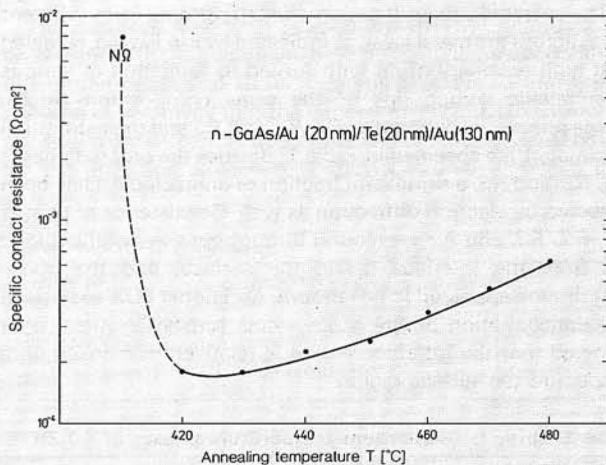

Fig. 2. Dependence of the specific contact resistance of GaAs/ /Au (20 nm)/Te (20 nm)/Au (130 nm) contacts annealed without caps on the temperature of heat treatment. Contacts annealed with a cap over this range of temperature were nonohmic

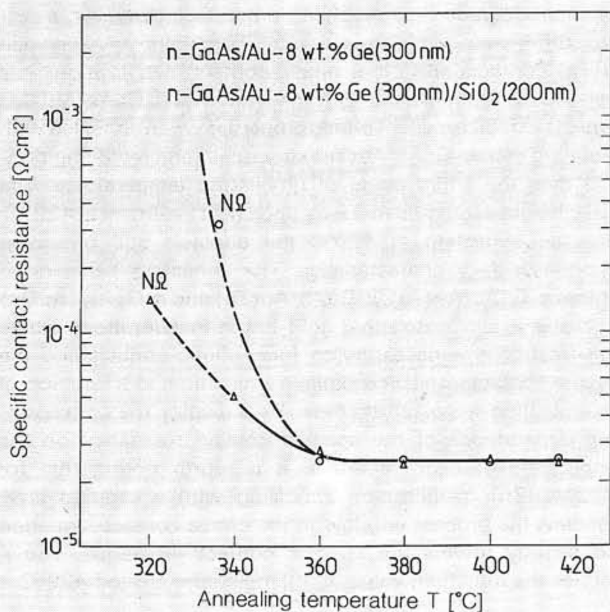

Fig. 3. Dependence of the specific contact resistance of GaAs/ /Au-8wt.% Ge (300 nm) contacts on the temperature of heat treatment

3.2. Microstructure

3.2.1. GaAs/Au/Zn/Au contacts

No sign of reaction between the metallization and GaAs has been observed in as-deposited contacts. However, in spite of sequential deposition of Au and Zn on GaAs, the Au/Zn/Au metallization did not exhibit a layered structure. RBS profiling indicated that Zn migrates predominantly into the inner Au film (see Fig. 5, in which the low-energy step of the Au spectrum of the as-deposited sample ensures for low-temperature interaction between Zn and Au). X-ray diffraction analysis showed that Au and Zn reacted to form the AuZn (50 at.% Zn) compound. After heating at about 100°C during sputter deposition of Al_2O_3 and/or the preparation of samples for TEM studies, room temperature phases of Au_3Zn were identified. Fig. 4a displays a cross-sectional TEM image of the as-deposited specimen. The metal layer consists of crystal grains (about 100 nm in diameter) oriented randomly with respect to the GaAs substrate.

The selected-area diffraction (SAD) patterns from different areas across the metal layer, as indicated by *x* in Fig. 4a, revealed that high reactivity of Zn with Au led to formation of various intermetallic compounds of the same composition Au_3Zn. These phases are denoted as *R1, R2,* and *R3* and their structural parameters are specified in Table 1. Besides the ordered phases *R1, R2,* and *R3,* a significant fraction of unreacted Au has been detected by electron diffraction as well. Coexistence of phases *R1, R2, R3,* and Au was found throughout the metal contact, i.e. from the interface up to the surface, and the phase distribution appeared to be random. Additional EDX analysis of the concentration profile of Zn atoms across the metal layer showed that the interface region is relatively rich in Zn with respect to the surface region.

Table 1. **Three possible room-temperature phases of Au_3Zn**

Structure type	Crystal system	Lattice parameters [Å]		
R1	Tetragonal	5.586	5.586	33.37
R2	Orthorombic	5.586	5.594	16.65
R3	Quasi-tetragonal	≈5.65	≈5.65	≈16.4

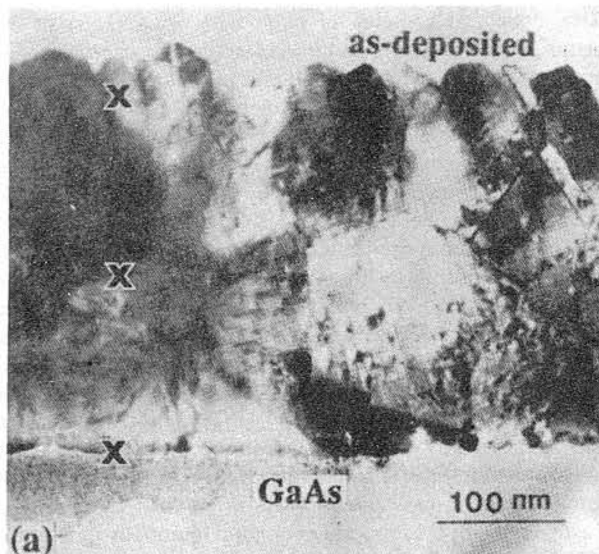

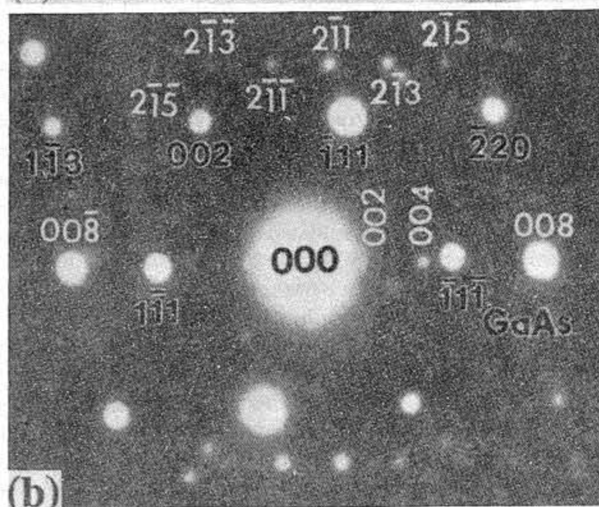

Fig. 4. (a) TEM micrograph showing the cross section of as-deposited GaAs/Au (40 nm)/Zn(40 nm)/Au (274 nm) contact. The marks *x* indicate the typical areas that have been analysed by electron diffraction and EDX. (b) SAD pattern taken from an interface area, showing reflections from the zone axes of GaAs [110] (black indices) and [120] of *R3* phase of $AuZn_3$ (white indices)

The effect of heat treatment on the structure of GaAs/Au/Zn/Au contact strongly depends on whether or not the capping layer is used during contact annealing. Contacts annealed in open system are characterized by rough surface and metal/semiconductor interface, whereas heat treatment in closed system produces contacts with smooth surface and interface. XRD analysis show that during thermal processing zinc reacts preferentially with gold forming Au_3Zn phases in both capless and cap-annealed contacts. Thermally activated interactions at GaAs/Au−Zn interface are dominated by the interaction between the remaining Au and GaAs.

Fig. 5. shows the RBS spectra of as-deposited and heat treated at 420°C for 3 min. GaAs/Au-Zn contacts, processed either with or without capping layer. The following characteristic features, resulting from the interaction of Au with GaAs, should be pointed out. They are a decrease in height of the Au spectrum and the overlap of signals from Au and GaAs for contacts annealed without capping layer, and a low-energy tail of Au spectra for cap-annealed contact. The above changes of the shape of the parts of the spectra corresponding to Au indicate the out-diffusion of gallium from GaAs into the corresponding Au-Zn metallization. In order to evaluate the

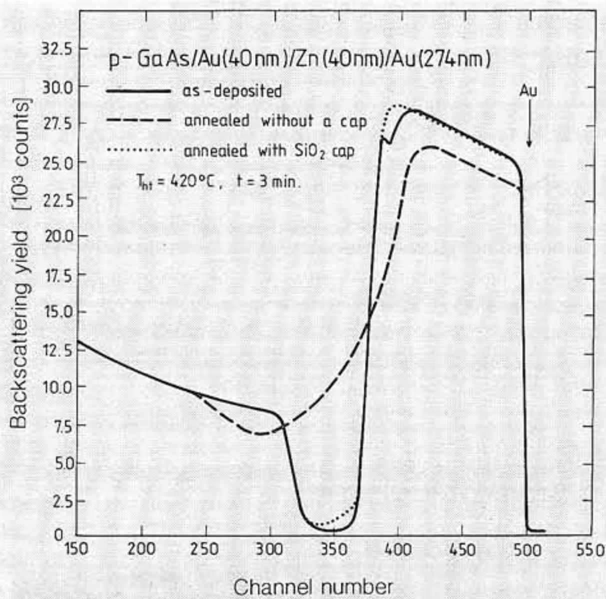

Fig. 5. The 2 MeV $^4He^+$ RBS spectra of as-deposited and annealed capless and capped GaAs/Au (40 nm)/Zn(40 nm)/Au (274 nm) contacts; heat treatment at 420°C for 3 min. in both cases. Capping layer removed before analysis

content of Ga atoms in the metallization, the computer simulation of RBS spectra using RUMP code were performed. The best fit was obtained for Ga content equal to 0.7% and 11% (i.e. $7.7 \cdot 10^{15}$ and $1.2 \cdot 10^{17}$ atoms/cm²) for cap- and capless-annealed contacts, respectively. The number of As atoms released from the same samples as determined by the Cr collector was $7.2 \cdot 10^{15}$ and $1.1 \cdot 10^{17}$ atoms/cm², respectively. The data on the outcome of *p*-GaAs/Au-Zn contact reaction are collected in Table 2. They prove that the extent of contact reaction Au-GaAs is reduced by the use of capping layer.

Fig. 6 displays the microstructure of cap-annealed GaAs/Au-Zn contact, as analysed by TEM. A XTEM image (Fig. 6a) shows that randomly oriented crystal grains in the metal layer exhibit about the same size as in as-deposited specimen, i.e. about 1100 nm in diameter. Electron diffraction of various areas, as marked by *x* in Fig. 6a, revealed that the metallization consisted of randomly distributed phases *R1, R2,* and *R3* of Au_3Zn and unreacted Au (α–AuGa). Fig. 4b shows a SAD pattern recorded from the interface area, where the reflections from the GaAs [110] zone axis (outlined black indices) can be readily recognized and the rest of diffraction spots can be indexed as the $[\bar{8}1\bar{2}]$ zone axis of Au_3Zn [*R1*] (white numbers). Additional EDX analysis of the concentration profile of Zn across the metallization showed that the distribution of Zn atoms became uniform as a result of heat treatment.

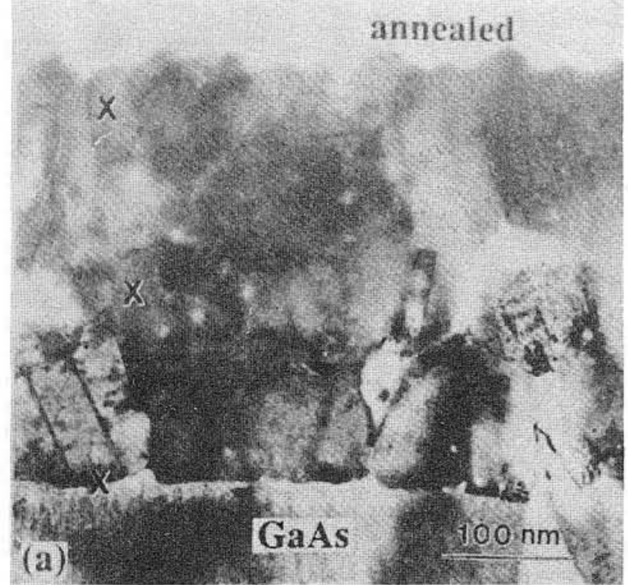

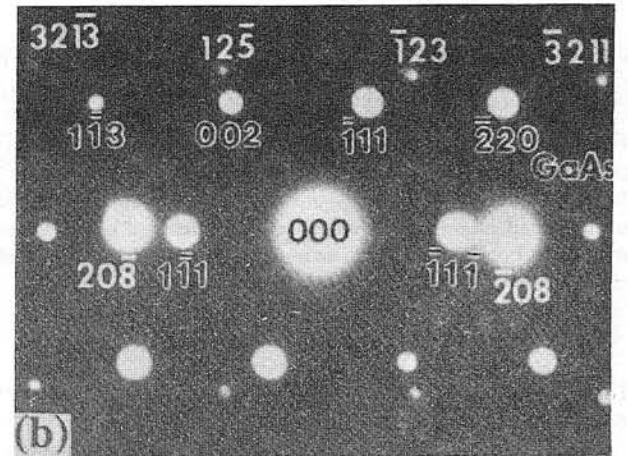

Fig. 6. a) TEM micrograph showing the cross section of GaAs/ /Au (40 nm)/Zn (40 nm)/Au (274 nm) contact annealed with capping layer at 420°C for 3 min. The marks *x* indicate the typical areas that have been analysed by electron diffraction and EDX. b) SAD pattern taken from an interface area, showing reflections from the zone axes of GaAs [110] (black indices) and $[\bar{8}1\bar{2}]$ of *R1* phase of Au_3Zn (white indices)

The interface was also studied by HREM. Although the crystal grains in the metal layer have no specific crystallographic orientation relative to GaAs, it is still possible to find grains oriented in such way that the lattice images of both GaAs and the Au_3Zn grains can be observed simultaneously. An example for the annealed specimen is shown in Fig. 7, where two

Table 2. **The influence of SiO_2 capping layer on the outcome of *p*-GaAs/Au/Zn/Au reaction**

Contact material thickness *d* [nm]	Heat treatment		Phase composition	Ga content in Au		As loss
	T [°C]	*t* [min.]		[at. %]	N_{Ga} [at/cm²]	N_{As} [at/cm²]
Au(40)/Zn(40)/Au(274)	as-deposit		Au AuZn	–	–	–
Au(40)/Zn(40)/Au(274)	420	3	Au_3Zn αAuGa	11	$1.2 \cdot 10^{17}$	$1.1 \cdot 10^{17}$
Au(40)/Zn(40)/Au(274)/SiO_2	420	3	Au_3Zn αAuGa	0.7	$7.4 \cdot 10^{15}$	$7.2 \cdot 10^{15}$

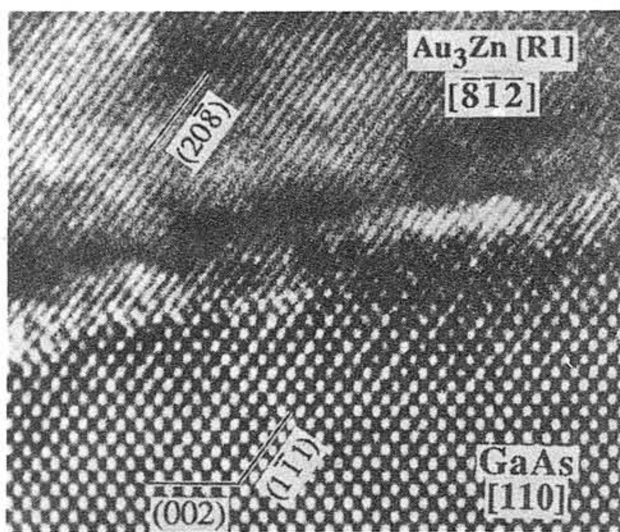

Fig. 7. HREM micrograph showing the interface between a crystal grain of *R1* phase of Au_3Zn and the GaAs substrate. The image is projected along GaAs[110]‖Au_3Zn [*R1*] [812]

interfacing crystals, phase *R1* of Au_3Zn and GaAs, exhibit the following relationship: *R1* $[\bar{8}1\bar{2}]$ ‖GaAs [110] and *R1*$(20\bar{8})$‖ GaAs$(1\bar{1}1)$; the corresponding diffraction pattern is given in Fig. 4b. In this case, the metal/GaAs interface displays a good coherency, i.e. continuation of atomic planes across the interface, and the atomic lattices of both materials appear almost undisturbed close to the interface, in spite of a rather large mismatch between the two materials ($d_{R1(208)} = 0.232$ nm and $d_{GaAs(1\bar{1}1)} = 0.326$ nm).

3.2.2. GaAs/Au/Te/Au contacts

No interaction between the metallization and GaAs has been observed in as-deposited contacts.

Fig. 8 gives the RBS spectrum and RUMP computer simulations of a GaAs/ 20 nm Au/ 20 nm Te/ 130 nm Au contact in as-deposited condition. According to RUMP simulations, no intermixing took place between Te and Au, and the layered metallization structure is preserved. XRD spectra have given clear diffraction lines of Te and Au without an indication of preferred orientation. The XTEM image of an as-deposited sample is given in Fig. 9. One can see that Te forms small islands on GaAs, covered by a continuous Au overlayer. Note that the Te islands on GaAs are composed of small crystals, of about 10 nm in diameter. The change from layered to island-like form of Te may be due to the heating up the contact to about 100°C during the specimen preparation for TEM studies.

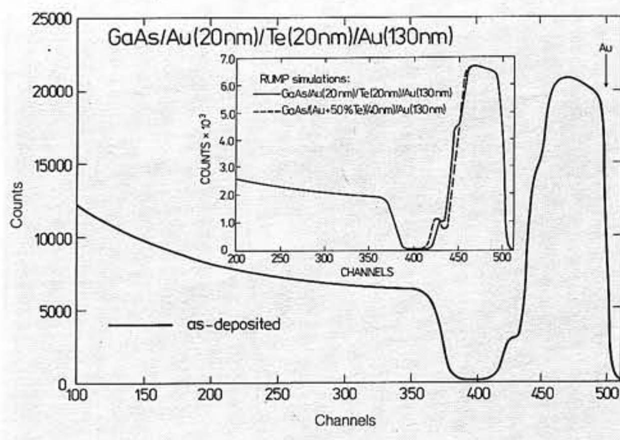

Fig. 8. The 2 MeV $^4He^+$ RBS spectra of as-deposited GaAs/Au (20 nm)/ /Te (20 nm)/Au (130 nm) contact

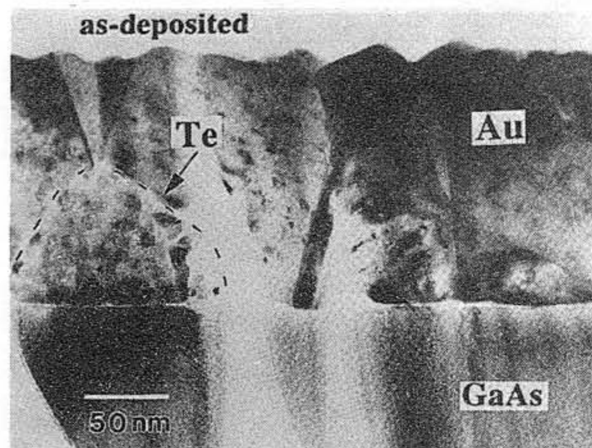

Fig. 9. TEM micrograph of as-deposited GaAs/Au (20 nm)/Te (20 nm)/ /Au (130 nm) contact

Annealing produces a dramatic change of contact microstructure. Here again, the outcome of contact reaction has been found to depend strongly on the use of a capping layer. The phase composition, as detected by XRD analysis, of GaAs/ /20 nm Au/20 nm Te/130 nm Au contact heat treated at 420°C for 3 min. and the volatile component losses are given in Table 3.

The outstanding effect of heating uncapped GaAs/Te/Au/Te contacts is the pronounced vaporization of both arsenic and tellurium. The use of an encapsulating layer enables suppressing the sublimation of volatile elements: tellurium losses have been reduced by two orders of magnitude, As losses decreased

Table 3. **The influence of Al_2O_3 capping layer on the outcome of *n*-GaAs/Au/Te/Au contact reaction**

Contact material thickness *d* [nm]	Heat treatment		Phase composition	Te loss		As loss
	T [°C]	*t* [min.]		*d* [at. %]	N_{Te} [at/cm^2]	N_{As} [at/cm^2]
Au(20)/Te(20)/Au(134)	as-deposit		Au Te	–	–	–
Au(20)/Te(20)/Au(134)	420	3	Au_3 Au_7Ga_2	15.4	$0.46 \cdot 10^{17}$	$1.39 \cdot 10^{17}$
Au(20)/Te(20)/Au(130)/Al_2O_2	420	3	Au Ga_2Te_3 As_2Te_3	0.2	$0.5 \cdot 10^{15}$	$17.3 \cdot 10^{15}$

by a factor more than 10. In the XRD spectrum of uncapped contacts Au diffraction lines together with reflections of Au_7Ga_2 have been observed. Contact annealed with a cap have shown clear diffraction lines of Au and Ga_2Te_3 as well as of the traces of As_2Te_3. Ga_2Te_3 was highly textured. The diffraction lines for Au revealed weak ⟨111⟩ preferred orientation.

Fig. 10 displays XTEM image of capped and uncapped Au(Te) contact, both annealed at 420°C for 3 min. For an uncapped contact the heat treatment results in the formation of a discontinuous $Au+Au_7Ga_2$ layer. When viewed in TEM cross section, this contact appears as small islands (black areas) on the top of the GaAs surface. Moreover, owing to interfacial reaction, these islands are seen to penetrate into the GaAs down to a depth of about 100 nm. No elemental Te or Te-related phases have been detected.

For contacts annealed with a cap the reaction products are basically Ga_2Te_3 (grey contrast) and Au crystals (black areas) which are laterally separated one from another by a distance of about 500 nm. The Au crystals are seen to protrude into GaAs down to a depth of approx. 50 nm, while the Ga_2Te_3 grains have a relatively flat interface with GaAs. Both the electron diffraction and the high-resolution imaging indicate that the Ga_2Te_3 grains are in epitaxy with the GaAs substrate with cube-on-cube orientation relationship: $Ga_2Te_3[110] \parallel GaAs[110]$ and $Ga_2Te_3(1\bar{1}1) \parallel GaAs(1\bar{1}1)$. Fig. 11 is a HREM image of Ga_2Te_3/GaAs interface, showing the continuation of atomic lattice planes across the interface. As for the Au grains, there is no defined orientation relationship between the Au and GaAs. Apart from Ga_2Te_3 and Au, we have also found (Fig. 12) a trace amount of monoclinic phase As_2Te_3, which is formed epitaxially in Ga_2Te_3 grains with the orientation relationship: $As_2Te_3[101] \parallel Ga_2Te_3[110]$ and $As_2Te_3(\bar{2}0\bar{2}) \parallel Ga_2Te_3(2\bar{2}0)$.

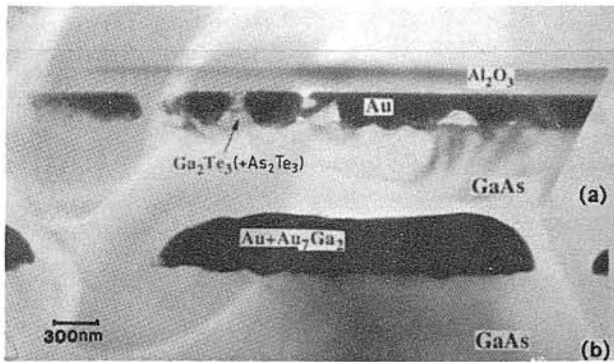

Fig. 10. TEM micrographs of GaAs/Au (20 nm)/Te (20 nm)/ /Au (130 nm) contacts annealed at 420°C for 3 min.: a) with an Al_2O_3 cap and b) without a cap

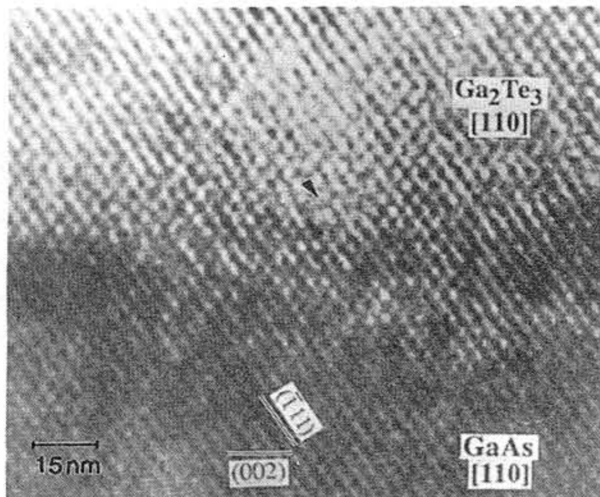

Fig. 11. HREM image of the interface between Ga_2Te_3 and GaAs as viewed along their [110] direction. The core region of a misfit dislocation is indicated by the arrow

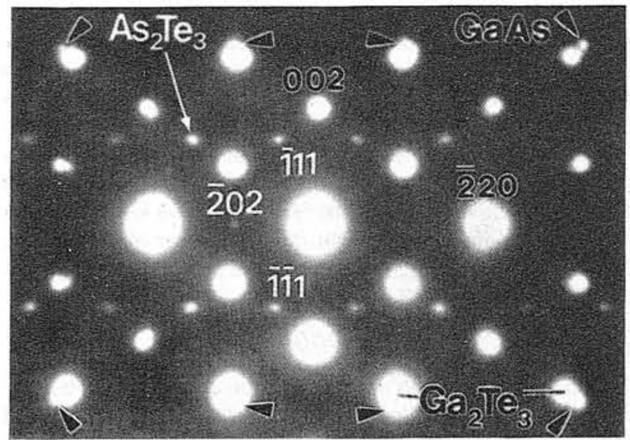

Fig. 12. SAD pattern taken from a Ga_2Te_3/GaAs interface area. The spots indexed with outlined black numbers correspond to reflections from the [110] zone axes of GaAs (indexed by arrows) and Ga_2Te_3, while the weak spots indexed with white numbers are reflections of the As_2Te_3 [101] zone axis. Note that only a trace amount of the monoclinic As^2Te_3 phase is found in the cap-annealed contact

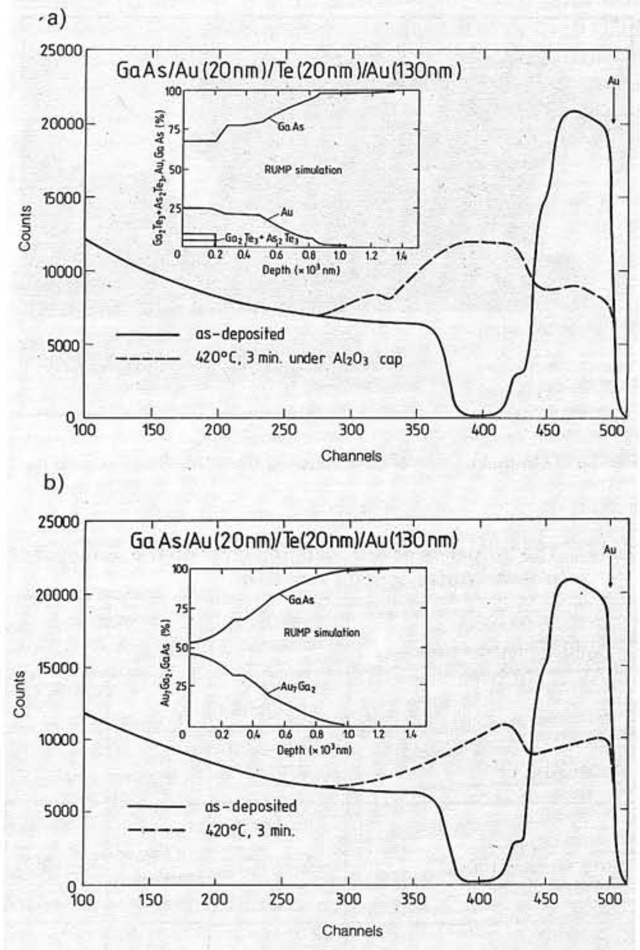

Fig. 13. The 2 MeV $^4He^+$ RBS spectra of GaAs/Au (20 nm)/ /Te (20 nm)/Au (130 nm) contacts annealed at 420°C for 3 min.: a) with an Al_2O_3 cap and b) without a cap

In Fig. 13 there are RBS profiles of GaAs/Au (20 nm)//Te (20 nm)/Au (130 nm) contacts, annealed at 420°C for 3 min. Because of the overlap of the signals, simulations were done for each of the spectra and used to determine the phase distribution in the contact region (insets in Fig. 13).

It should be mentioned that the formation of a discontinuous metallization in Au-Te contacts annealed without capping layer (Fig. 2) results in the decrease of the effective ohmic contact area. Thus, we can expect that the true values of the specific contact resistance are lower than those presented in Fig. 2.

3.2.3. GaAs/Au(Ge) contacts

No interaction between the metallization and GaAs and between the metallization constituents themselves has been observed in as-deposited contacts. The distribution of Ge throughout the metallization, as indicated by SIMS analysis (Fig. 15a) is homogeneous. The XTEM image of an as-deposited specimen (Fig. 14) indicates that the metal layer consists of separate Ge grains embedded in continuous Au film.

Annealing activates contact reaction between metallization and GaAs and the most interesting results is a little effect of capping layer on the outcome of contact reaction GaAs/Au(Ge).

Compositional analysis of Cr-collectors heated in contact with GaAs/Au-8wt.%Ge (300 nm) structures show that vaporization of As is small (see Table 4). The SIMS analysis indicate that arsenic is bounded in the metallization after contact annealing. This is clearly seen in Fig. 15, where composition

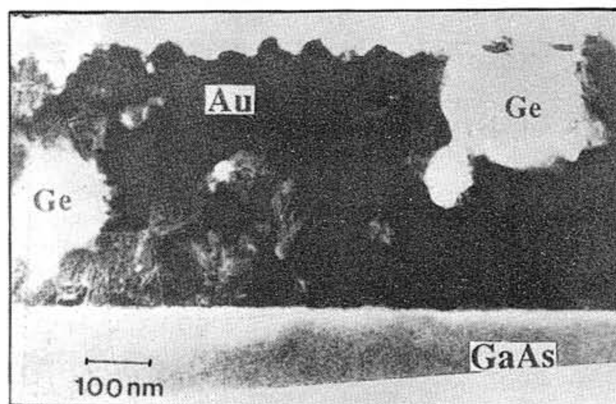

Fig. 14. TEM micrograph of as-deposited GaAs/Au-8wt.% Ge contact

Table 4. **The influence of SiO_2 capping layer on the outcome of *n*-GaAs/AuGe contact reaction**

Contact material thickness *d* [nm]	Heat tratment *T* [°C]	Heat tratment *t* [min.]	Phase tratment	As loss N_{As} [at/cm²]
Au wt.%Ge (300)	as-deposited		Au Ge	–
Au-8 wt.%Ge (300)	420	3	Au Ge AuGeAs Au_2Ga	$5 \cdot 10^{16}$
Au-8 wt.%Ge (300)/SiO_2	420	3	Au Ge AuGeAs Au_2Ga	$<10^{15}$

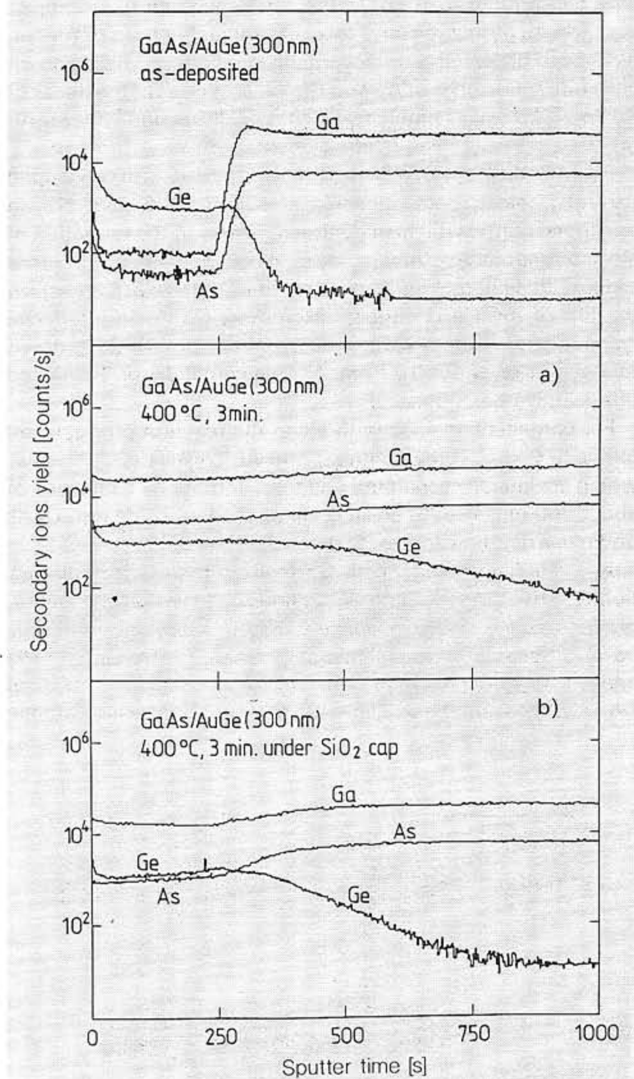

Fig. 15. SIMS depth profiles of as-deposited and annealed at 420°C for 3 min. GaAs/Au-8wt.%Ge contacts: a) heat treatment with an Al_2O_3 cap and b) without a cap

profiles of the corresponding GaAs/Au(Ge) contacts involves As signals registered throughout the whole metallization. The XRD analysis gave evidence for the formation of AuGeAs phase, with lattice parameters reported previously by Auvray et al. [21].

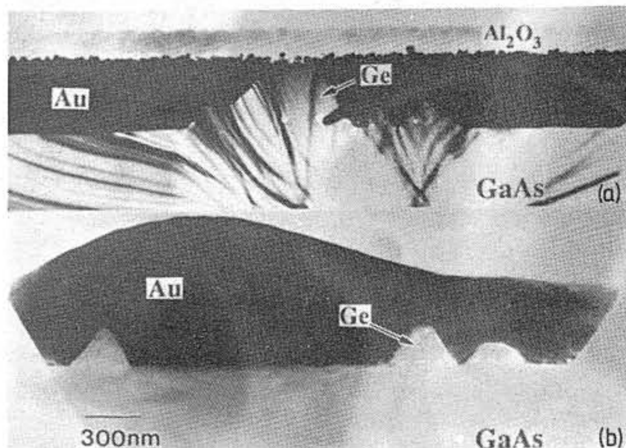

Fig. 16. TEM micrographs of GaAs/Au-8wt.%Ge contacts annealed at 420°C for 3 min.: a) with an Al_2O_3 cap and b) without a cap

Fig. 16 shows the XTEM micrographs of the structure of GaAs/Au(Ge) contacts annealed at 420°C with and without a cap. In both cases, annealing results in triangle-shaped Ge grains; most of them are covered by the Au overlayer. All the Ge grains were formed by epitaxial regrowth of Ge on the GaAs substrate. The Au(Ge)/GaAs interface remains microscopically flat for both capped and uncapped anneals. The only difference is that the capped contact exhibits a smooth surface, while the surface of the uncapped ones is rough.

The data on the outcome of contact reaction in GaAs/Au-Ge contacts are summarized in Table 4.

4. Conclusions

The results of electrical characterization of *p*-GaAs/Au/Zn/Au, *n*-GaAs/Au/Te/Au and *n*-GaAs/Au-Ge contacts under heat treatment indicate that any of these systems when treated under proper annealing conditions presents ohmic behaviour. Having in mind the kinetics of Au/GaAs reaction in open and closed configurations, the comparison of cap- and capless-annealed contacts testify in favour of the doping model of ohmic contact formation. Zn seems to play the role of *p*-type dopant, Te and Ge seems to take the role of *n*-type dopants. When annealing is performed in open system, both gallium and arsenic vacancies become available and Zn, Ge, and Te can occupy appropriate sites and form ohmic contacts. In closed system, the reaction of Au with GaAs produces preferentially Ga vacancies and only Zn or Ge are able to play electrically active role. Thus when the system is closed by an insulating cap, reducing the availability of As sites, the GaAs/Au-Te contact is nonohmic.

Metallurgical studies give evidence that the interfacial phenomena governing the ohmic behavior are more complex as to be described by the drive of dopants from the metallization into the underlying semiconductor. The outstanding feature of contact reaction of Au-Zn, Au-Te, and Au-Ge metallizations with GaAs is the dissimilarity of metallurgical behaviour of three doping elements involved. Also of importance is the influence of cap-annealing on microstructure of GaAs/Au-Zn, GaAs/Au-Te, and GaAs/Au-Ge ohmic contacts.

There is no doubt that the success and the ultimate shortcomings of gold-based metallizations are strongly related to interactions in the Au/GaAs system and this reaction is strongly dependent on the use of capping layer during contact annealing. However, additional elements introduced into the Au metallization change the kinetics of reaction between Au and GaAs. The development and the final microstructure of the contact region strongly depend on particular element (its reactivity with Au and GaAs) and annealing conditions (the use of capping layer).

As for Au-Zn metallization our results show that Zn reacts preferentially with Au and thermally activated interactions at GaAs/Au-Zn interface are dominated by the interaction between Au and GaAs. In an open system, vaporization of As is the driving force of the interfacial reaction and causes extended decomposition of GaAs and the formation of metallic protrusions. The presence of a capping layer limits the interaction of Au with GaAs. It is important to note that contact reaction occurring in a very thin interfacial region is sufficient to produce ohmic behaviour.

As for Au-Te metallization, our results indicate that Te does not react with Au neither in open nor in closed systems. The reactivity of Te with GaAs depends on whether a cap is used or not. At the temperature of ohmic contact formation, Te is highly volatile and an overlayer of Au only slightly restrains the sublimation of Te from GaAs/Au/Te/Au contact annealed without a cap. In these structures the contact reaction is dominated by the Au-GaAs interaction and metallization forms a discontinuous layer protruding in the GaAs. It is difficult to speculate on the possible population of Ga and As vacancies and their occupation by Te atoms in a so heavily reacted contact with an inhomogeneous interface. However, it should be stressed that the microstructure resulting from Au-GaAs reaction, containing some Te, without any detectable product of Te-GaAs interaction, exhibits ohmic behavior. In closed system, suppression of As vaporization restrains the Au-GaAs reaction, while reduction of Te sublimation activates the Te-GaAs reaction. Ga_2Te_3 and As_2Te_3 are the main products of the interaction, apart from unreacted Au and small quantities of Au_7Ga_2. Such interactions, in spite of that both Ga_2Te_3 and As_2Te_3 are narrow-bandgap semiconductors, do not lead to the formation of ohmic contacts to *n*-GaAs.

The metallurgy of Au-Ge contacts presents another picture. Upon annealing both, in open and closed configurations, Ge partly regrows on GaAs surface and partly reacts with Au and As, forming AuGeAs phase. That is why the effect of capping layer on contact reaction is less pronounced.

The results as a whole, indicate that the use of Au as the main component of the metallization inevitably implies the choice of such kind of dopants that are electrically active when placed on Ga sites. They also suggest that Au-based ohmic contacts are more controllable than commonly believed. In particular, they show that the formation of metallic protrusion, specific for uncapped contacts, can be avoided.

Acknowledgement

The research was supported by State Committee for Scientific Research (Grant No. 8 8026 92 03), and SDIO/Innovative Science and Technology program administrated through ONR under contract N00014-86-K-0668. The microscopy studies were performed employing the facilities of the National Center for Electron Microscopy founded by the U.S. Department of Energy under contract No. DE-AC03-76SF00098.

References

1. *A. Piotrowska, A. Guivarc'h, G. Pelous:* Solid-State Electron., **26** (1983) p. 179.
2. *C.J. Palmstrom, D.V. Morgan:* in: Gallium Arsenide (*M. J. Howes* and *D.V. Morgan* – eds.). J. Wiley, Chichester 1985, p. 195.
3. *G.Y. Robinson:* in: Physics and Chemistry of III-V Compound Semiconductor Interfaces (*C. W. Wilmsen* –ed.). Plenum Press, New York 1985, p. 73.
4. *T. Sands:* Mater. Sci. Eng., **B1** (1989) p. 289.
5. *A. Piotrowska, E. Kamińska:* Thin Solid Films, **193/194** (1990) p. 511.
6. *M. Murakami:* Mater. Sci. Rep., **5** (1990) p. 273.
7. *R.S. Popovic:* Solid-State Electron., **21** (1978) p. 1133.
8. *R.P. Gupta, W.S. Khokle:* Solid-State Electron., **28** (1985) p. 823.
9. *W. Dingfen, W. Dening, K. Heime:* Solid-State Electron., **29** (1986) p. 489.
10. *A.K. Kulkarni, C. Lai:* Thin Solid Films, **164** (1988) p. 435.
11. *T. Sebestyen:* Solid-State Electron., **25** (1982) p. 543.
12. *D. Kirillov, Y. Chung:* Appl. Phys. Lett., **51** (1987) p. 846.
13. *A. Illiadis:* J. Vac. Sci. Technol., **B5** (1987) p. 1340.
14. *J.F. McGilp:* J. Mater. Res., **2** (1987) p. 516.
15. *A. Piotrowska* et al.: Acta Phys. Pol., **80** (1991) p. 457.
16. *A. Piotrowska* et al.: J. Appl. Phys., **73** (1993) p. 4404.
17. *R. Beyers, K.B. Kim, R. Sinclair:* J. Appl. Phys., **61** (1987) p. 2195.
18. *J.H. Pugh, R.S. Williams:* J. Mater. Res., **1** (1986) p. 343.
19. *A. Barcz, E. Kamińska, A. Piotrowska:* Thin Solid Films, **149** (1987) p. 251.
20. *E. Kuphal:* Solid-State Electron., **24** (1981) p. 69.
21. *P. Auvray* et al.: Thin Solid Films, **127** (1985) p. 39.